Journal of Renewable Energy and Sustainable Development (RESD) Volume 10, Issue 2, December 2024 - ISSN 2356-8569
http://dx.doi.org/10.21622/RESD.2024.10.2.1050

Received on, 06 October 2024 Accepted on, 20 November 2024 Published on, 27 November 2024

Laser-Enhanced Hydrogen Production: Designing a PEC Cell Photoanode with an Exclusive Dye Material for Superior Efficiency

Sally A. Al-Ani [1*], and Mohamed K. Dhahir [2]

[1,2] Institute of Laser for Postgraduate Studies, University of Baghdad, Al-Jadriya, Baghdad, Iraq

Sally.Abdulrazaq1101a@ilps.uobaghdad.edu.iq, mohammed@ilps.uobaghdad.edu.iq

ABSTRACT

This study presents a novel approach to enhancing the performance of photoelectrochemical (PEC) cells by leveraging laser illumination with the assistance of a UV source as a superior alternative to conventional solar light. A distinct photoanode was fabricated using a unique dye material, strategically designed with multiple layers to optimize light absorption across the ultraviolet (UV), visible (VIS), and near-infrared (NIR) regions. By matching the incident laser wavelength with the photoanode absorption peaks, the system achieved exceptional photocurrent densities, outperforming conventional solar illumination which is represented by a LED source. The photoanode was meticulously fabricated by drop-casting carefully selected materials onto a fluorine-doped tin oxide (FTO) substrate consisted of cerium oxide (CeO2) nanoparticles, copper (Cu) nanoparticles, and the exclusive material (Epolight™ 1178) as a novel dye sensitizer used in this sector. Structural and compositional analyses were conducted using X-ray diffraction (XRD), energy-dispersive X-ray spectroscopy (EDS), and field-emission scanning electron microscopy (FE-SEM). Optical properties were evaluated using a UV-VIS-NIR spectrophotometer, confirming absorption peaks at (357, 473, 634, and 857) nm spanning UV, VIS, and NIR regions and enhancing the PEC cell hydrogen generation efficiency. Photoelectrochemical measurements were carried out by linear sweep voltammetry in the dark and under illumination condition AM 1.5 G of 100 mW/cm2. Comparative analysis between laser-illuminated and traditional light-illuminated systems demonstrates a notable increase in hydrogen production efficiency in the laser-driven setup from 8.2% to 33.2%. This research highlights the potential of laser-assisted PEC technology as a pathway to overcoming the limitations of traditional solar energy systems, contributing to advancements in sustainable energy solutions.

Index-words: *Water splitting, Hydrogen production, Laser application, PEC photoanode.*

I. INTRODUCTION

The global energy crisis and the environmental impacts of fossil fuels have intensified the search for sustainable and clean energy sources. Among the many alternatives, hydrogen has emerged as a promising energy carrier due to its high energy density and zero-carbon emissions when utilized in fuel cells. As the ideal source is water, one of the most efficient methods for producing hydrogen is through photoelectrochemical (PEC) water splitting, which uses sunlight to drive the chemical reaction that generates hydrogen from water [1,2]. However, the efficiency of PEC systems is often limited by the photoanode light absorption, charge separation, and stability under operational conditions [3]. For a PEC cell that typically consists of photoelectrode as working electrode, which could be an n-type (photoanode) or p-type (photocathode) semiconductor, and a counter electrode (CE), that is usually a metal (e.g., Pt.) immersed in a suitable electrolyte [4,5], when light hits the photoanode, it absorbs the energy and generates electron-hole pairs that drive the water-splitting reaction. The rate of absorption of sunlight through photoanode material is considered the key to hydrogen production increment. It is known that only 4% of the sunlight on Earth is UV. Therefore, the photo response of the working electrode (photoanode) absorption must extend to the visible light or NIR area to attain optimal efficiency [6]. To address these challenges, various photoanode materials have been explored. Cerium dioxide (CeO_2) which is often known as ceria is an n-type semiconductor has garnered attention due to its excellent stability, high oxygen storage capacity, and tuneable optical properties [7]. As the potential of CB and VB in CeO_2 follow the requirements of hydrogen generation, when the CB is more negative than the potential of hydrogen evolution and the VB potential is more positive than the potential of

oxygen evolution. Moreover, cerium oxide exhibits strong absorption in the UV region, and it is highly transparent in the visible region (400–800 nm) and near IR region [8]. Another important characteristic is the cost consideration because it is inexpensive [9]. However, the relatively large bandgap of CeO_2 limits its absorption of visible light. To improve its light-harvesting efficiency, CeO_2 has been modified with other materials with various dopants and co-catalysts or in the form of thin film composite. It is also worth noting that the kind of deposition procedure often affects the properties and activity of thin films. Although there are other methods used, the Drop-Cast process is a quick, simple, and affordable non-vacuum method [10]. Furthermore, the number of layers can regulate the final thickness. It is like spin coating technique, but no substrate spinning is required [11]. In thin films, when the layer of metal oxide encounters the metallic photo absorber, a Schottky junction is formed which sometimes known as a semiconductor–metal [12-14].

Among metallic materials the Copper Cu is one of the most abundant elements found on Earth. It has played an important part in history, given its many properties, like good electrical and thermal conductivity, high corrosion resistance and increased malleability [15]. Metallic nanoparticles (NP) are gaining attention from chemists because of their unique characteristics, which include a large surface area and remarkable surface activity that offers superior catalytic, optical, and electrical abilities[16]. Moreover, it is cheap and widely available, thus obtaining Cu NPs is cost effective [17]. On the other hand, Cu nanoparticles have excellent plasmonic properties including the surface plasmon resonance effect that spans the UV–visible region of the optical spectrum [18,19] .

Using materials with charges removal and harness light outside of the ultraviolet (UV) range are the two most difficult problems. Because visible light makes up to 47% of sunshine and UV radiation only contributes for 5-7%, the remaining energy in sunlight falls in the near-infrared (IR) portion of the electromagnetic spectrum. For hydrogen production to be achieved in the near-infrared region of solar energy, the dye molecules that are used as the light absorber are essential. Furthermore, as the dye molecule modification may change the photon energy absorbed, suitable selection should be used in dye-sensitized photocatalytic water-splitting systems [20]. While traditional PEC systems rely on solar illumination, the use of laser light has emerged as a novel approach to further enhance the efficiency of PEC cells. Laser illumination offers several advantages, including monochromatic and high-intensity light that can be precisely tuned to match the absorption properties of the photoanode materials.

This study investigates the effect of laser illumination on hydrogen production by designing a distinct PEC cell photoanode incorporating CeO_2, Cu nanoparticles, and an exclusive dye material. The use of laser light is hypothesized to improve light absorption and charge separation, ultimately leading to higher hydrogen production efficiency. The influence of laser light on the performance of this photoanode is compared to traditional solar illumination, providing insights into the potential of laser-assisted PEC technology for hydrogen generation.

A. Experimental Fabrication of the Photoanode (P)

The photoanode is a multi-junction thin film that consists of a clean, (1 x 1) cm^2 piece of glass coated in fluorine tin oxide (FTO) substrate, a layer of CeO_2 nanoparticles, a layer of Cu nanoparticles, and a layer of (Epolight™1178) dye material as [CeO_2(NP)/Cu(NP)/Epolight™ 1178]. CeO_2 is a 99.9% pure powdered nanoparticle that was bought from (HONGWUNEWMATERIAL) with particle size of 50 nm. Cu (NP), the 99.99% pure Cu nanoparticles are supplied by (Nanjing Nano Technology Co., ltd.) with particle size of 10-30 nm. The Epolight™ 1178 is a brown dye substance purchased from the USA Epolin Company (Broad IR absorber, suitable for coatings, melting point: 210 - 213°C, and the peak wavelength λ max: 1073 nm). Deionized (DI) water is used as the solvent for all suspensions.

A 0.2 g quantity of cerium dioxide (CeO_2) nanoparticles is dispersed in 25 mL of deionized (DI) water to form the suspension. The mixture is magnetically stirred for 1 hour at room temperature to ensure proper dispersion of CeO_2 particles. A micropipette is used to drop-casting (3) drops of the CeO_2 suspension onto the cleaned FTO substrate to form the first layer. Then, the film is allowed to dry on a hot plate. Using the same process in the first layer formation, the second layer is formed by dispersing 0.2 g of copper (NP) in 25 mL of deionized (DI) water. The suspension is stirred continuously for one hour to achieve a uniform mixture. Following the preparation of the Cu (NP) suspension, (8) drops

Volume 10, Issue 2, December 2024 - ISSN 2356-8569
http://dx.doi.org/10.21622/RESD.2024.10.2.1050

are drop-casted onto the pre-formed CeO_2 layer and dried on a hot plate. For the final layer, a dye material Epolight™ 1178 (0.3) g is dissolved in 25 mL DI and stirred for (2) hours to form a stable dye solution using a micropipette, (5) drops of the dye solution are cast onto the previously drop casted CeO_2/Cu bilayer and dried on a hot plate. The formation details are provided in Table I and Fig. 1 displays a simple diagram showing how a manufactured thin film is used as a PEC cell photoanode.

TABLE I
MATERIALS, WEIGHTS, NUMBER OF DROPS THAT ARE USED IN THE FABRICATION OF THE (P)PHOTOANODE.

The designed photoanode (P)	Layer arrangement	Selected Material	Material weight (g)	DI mL	No. of Drops
[CeO_2(NP)/Cu(NP)/Epolight™ 1178]	1st layer	CeO_2(NP)	0.2	25	3
	2nd layer	Cu (NP)	0.2	25	8
	3rd layer	Epolight™ 1178	0.3	25	5

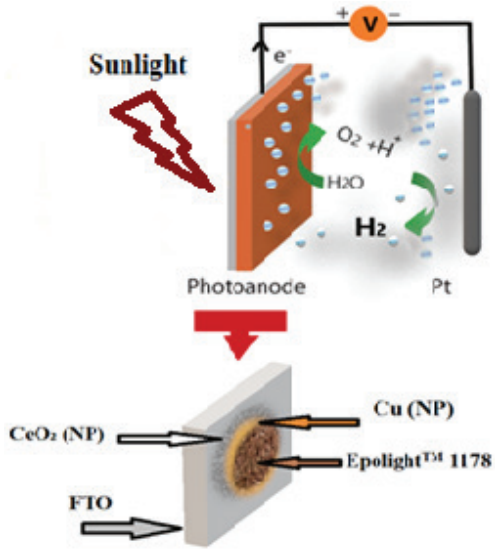

Fig.1. Diagram showing how a manufactured thin film is used as a PEC cell photoanode

II. MATERIALS CHARACTERIZATION

A. X-Ray Diffraction Measurement (XRD)

XRD characterization is used for materials identification to confirm their structural properties. The X-ray diffraction patterns of CeO_2 (NP) and Cu (NP) are obtained using (Aeris – Malvern Panalytical's X-ray diffractometer). The scanning is over the required range for 2Θ values (15 – 75) o with ± 0.02° 2θ peak position accuracy. Peaks of crystalline phases are compared with those of standard compounds of the materials with previous research.

B. EDS Characterization

To understand the elemental composition of the Epolight™ 1178 dye material, Axia ChemiSEM is used to gather energy-dispersive X-ray spectroscopy EDS measurement data. Moreover, top-view SEM and the corresponding EDS mapping images of Epolight™ 1178 are gathered to demonstrate the elements distribution and examine the intense presence of any element particles within the material.

1. Thickness and Cross-sectional Measurements

The morphological characteristics of the designed photoanode are detected using FE-SEM InspectTM F50. Cross-sectional FE-SEM images are used to indicate the thickness of this photoanode.

2. Optical Analysis

To investigate the optical properties of the P photoanode, the UV-VIS-NIR -1800 (SHIMADZU, Japan) spectrophotometer is used. This instrument is computerized with a CRT screen and keyboard for operating the input value. The absorption spectra are characterized with wavelength range of (190–1100) nm.

3. Photoelectrochemical Characteristics

To study the photoelectrochemical performances of the P photoanode as an efficient photonode, it is tested by an electrochemical workstation (ER466, EDAQ company Australia, potentiostat). Ag/AgCl serves as the reference electrode, Pt serves as the counter electrode, and the designed photoanode (P) serves as the working electrode in the three-electrode system. Regular testing at room temperature uses a 125 mL quartz cell with 2g KOH in DI water with PH (9), which serves as the electrolyte. The linear sweep voltammetry curve is recorded with a scan

Volume 10, Issue 2, December 2024 - ISSN 2356-8569
http://dx.doi.org/10.21622/RESD.2024.10.2.1050

starting at (0-1) V versus (Ag/AgCl). J-V curves are obtained at a rate of (100) mW/s and at a frequency of (20) kHz at the corresponding program. The light emitting diode (LED) Source (42 W, Zethors H7) is used to illuminate the photoanode under AM 1.5 G condition of (100) mW/cm^2.

III. RESULTS AND DISCUSSION

The structural information of CeO_2 (NP) and Cu (NP) is characterized by a powder X-ray diffraction (XRD) pattern. Fig. 2 displays the pattern of the CeO_2 nanoparticles. It reveals all of the major peaks of CeO_2 which coincides with lattice planes (111), (200), (220), (311), (222), and (400) and are positioned at 2θ = 28.55 °, 33.08 °, 47.51 °, 56.31 °, 59.10 ° and 69.41 °. These findings are identified using the standard data (JCPDS Card No. 34-0394).

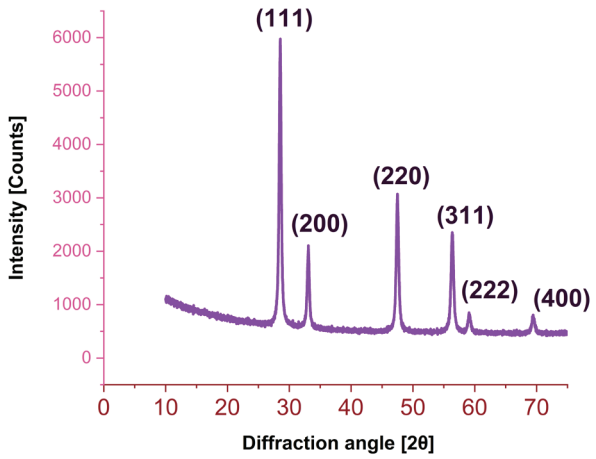

Fig. 2. XRD pattern of CeO_2 (NP)

An XRD diffractogram of copper nanoparticles is shown in Fig. 3. The typical lines indexed as (111), (200), and (220) that are found at diffraction angles of 43.30°, 50.42° and 74.10°, respectively, correspond to the copper nanoparticles diffraction peaks which are identified by using the standard data (JCPDS Card No. 04-0838). A broad diffraction peak of cuprite (111) is observed at a diffraction angle of 36.2°. Those diffraction peaks are similar in terms of angular positions to that of FCC pure bulk copper crystalline peaks but are relatively broad, as the mean size of the particles is of the order of nanometers [21].

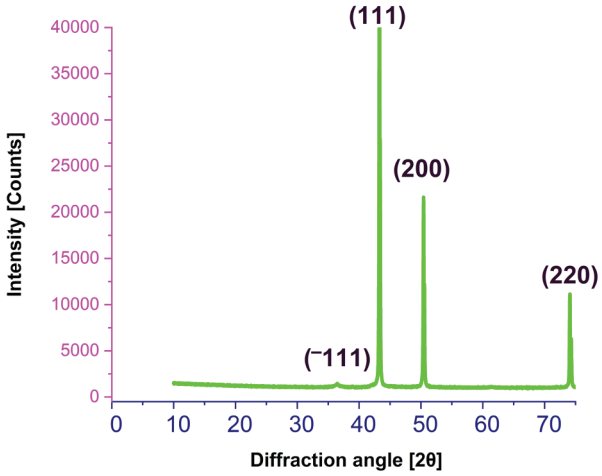

Fig. 3. XRD pattern of Cu (NP)

The near Infrared Epolight™ 1178 Dye material is a Broad IR absorber with Peak wavelength, λ max: 1073 nm as shown in Fig. 4(a), while Fig. 4(b) shows the EDS elemental analysis data of the dye material. The result detects the occurrence of the elements Carbon, Fluorine, Aluminum and Antimony (Sb) with high atomic percentage to Carbon reach to (76.4%). The strong presence of the Carbon is one of the reasons that make Epolight™ 1178 high NIR absorber [22]. Top-view SEM and the corresponding EDS mapping images of Epolight™1178 are represented in Fig. 4(c).

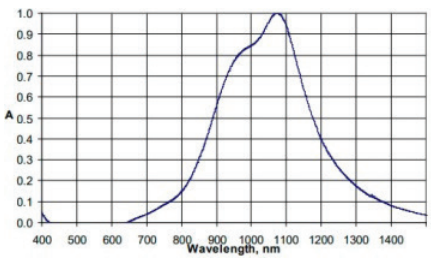

(a)

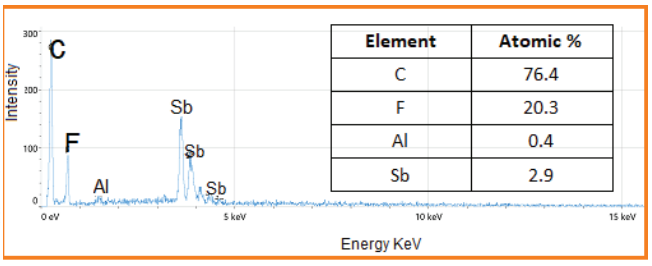

Element	Atomic %
C	76.4
F	20.3
Al	0.4
Sb	2.9

(b)

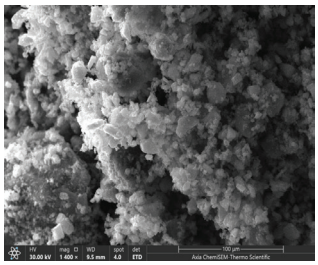

(c)

Fig. 4. (a) The absorption spectrum of Epolight™ 1178 indicates the peak at 1073 nm; (b) EDS spectral and elemental analysis data of Epolight™ 1178; and (c) SEM image of Epolight™ 1178

Volume 10, Issue 2, December 2024 - ISSN 2356-8569
http://dx.doi.org/10.21622/RESD.2024.10.2.1050

Using Field emission scanning electron microscopy FE-SEM, cross-sectional images of the P fabricated photoanode [FTO/CeO_2(NP)/Cu(NP)/ Epolight™ 1178] are acquired and displayed in Fig. 5. As can be seen from the figure, the thickness of the top layers (Cu(NP)/ Epolight™ 1178) varied from (9.51 to 11.79) µm, but the initial layer (FTO/CeO_2(NP) is only (0.457) µm thick, meaning that the overall thickness of the layers is approximately (9.9 – 12.2) µm.

It should be mentioned that when the suspension of Epolite™ 1178 in DI is drop-casted over the preceding layer of Cu (NP), the so-called coffee ring effect (CRE) is seen. Deegan et al. [23] make notable observations as they emphasize and provide an interpretation of this phenomenon. When the suspended particles form a ring-shaped pattern, the concentration is near the edges instead of in the center. The (CRE) is known for its detrimental effects since it tampers with the generally uniform dispersion of particles [24]. The surface tension force of Cu (NP) is the primary cause of (CRE) manifestation in the P formation. To address this problem, higher deposits are required, but it is also critical to take the thin film thickness limit into account. Furthermore, the dye material (Epolight™ 1178) is micrometer sized. Therefore, it is required to thin the first layer down and create a balance to obtain the ideal thickness of the electrode which ranges between (8-12) µm to achieve maximal absorption. The decreased thickness of the material in a film with a thickness of less than 8 µm results in less light absorption. The films thicker than 12 µm result in increased recombination as the charge carriers must diffuse across the additional layers [25].

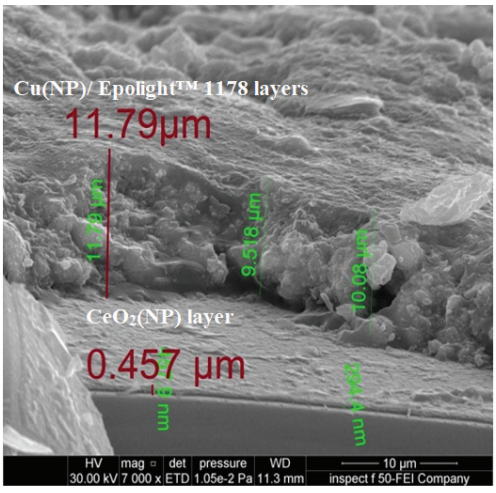

Fig. 5. FE-SEM, cross-sectional image of the P photoanode [FTO/CeO_2(NP)/Cu(NP)/ Epolight™ 1178)

The absorption spectra of the fabricated photoanode P thin film reveal an optimal light absorption, demonstrated by the clear peaks at Fig. 6 A, which illustrates its significance. Using the unique Epolight™ 1178 dye compound which has a λ max at 1073 nm (as mentioned in Fig. 4(a), previously, ensures the absorption towards the NIR region that is crucial for creating an effective photoanode. This can be seen in Fig. 6(b), with the clear absorption peak at (857) nm related to this dye material. On the other hand, there is a strong absorption below 400 nm in the thin film, with a peak at (357) nm displayed in the Fig. 6(a) which is related to cerium oxide nanoparticles that generally exhibit significant absorption peaks in the UV region [26], while the rest of the peaks in the same figure are (473 and 634) nm. They belong to the Cu nanoparticles, which form the second layer of the P photoanode. This may be consistent with studies that are published regarding Cu (NP) absorption peak, which is located at 570 nm [27,28].

Fig. 6 C indicates that the 473 nm is a more intensive peak than the other of 634 nm. Higher efficiency is associated with the appearance of many peaks in the visible region of the absorption spectrum, which are connected to the incorporation of a dielectric semiconductor CeO_2 with a plasmonic Cu nanostructure [29,30]. Because boosting light absorption through metallic enhancement is one method that surfaces plasmon resonance (SPR) that may increase semiconductor photocatalytic activity [31].

Based on these findings, it can be said that the materials chosen for the designed photoanode in addition to its ideal thickness allowed for maximal absorption to be regulated and attained for covering the three regions of UV, VIS and NIR, which provides a fertile ground for the success of any photoanode for a PEC cell.

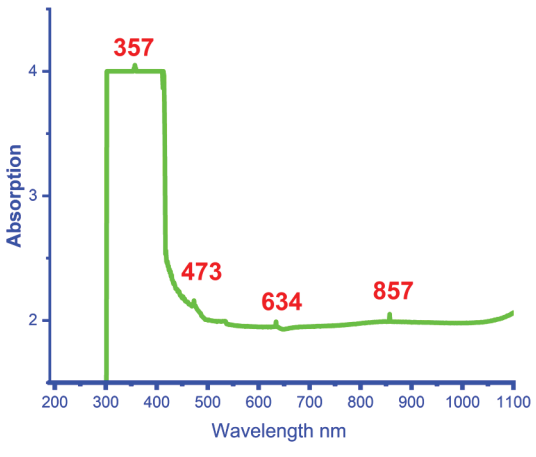

(a)

Volume 10, Issue 2, December 2024 - ISSN 2356-8569
http://dx.doi.org/10.21622/RESD.2024.10.2.1050

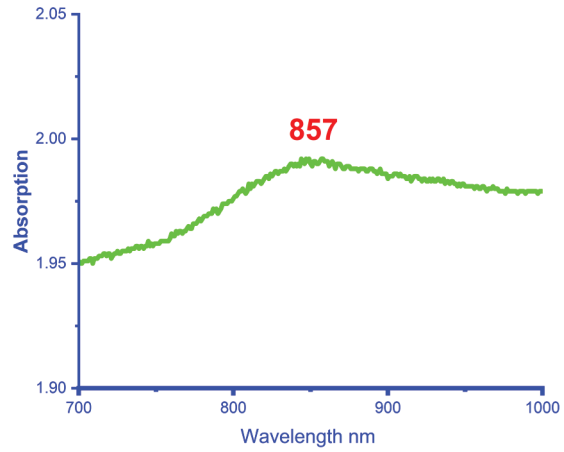

(b)

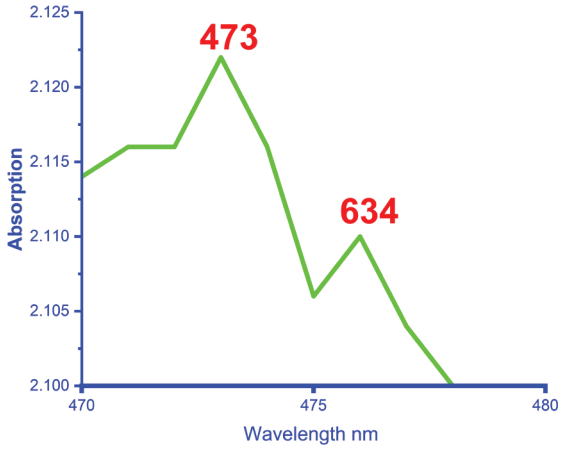

(c)

Fig. 6. Absorption spectrum: (a) of the (P) fabrictaed photoanode [CeO_2(NP)/Cu(NP)/Epolight™1178] (b) a close view of the NIR region of P; (c) a close view of the VIS region of P

Optical properties and band alignment of the photoelectrode are essential factors for enhancing PEC performance, the band gap energy (Eg) of the thin film is computed from the absorption data of the P photoanode with comparison to a thin film (S) fabricated just with the first layer of CeO_2 nanoparticles for indicating the change in band gap after the addition of the other materials layers. Using the Tauc's equation 1 [32] :

$$\alpha h\nu = A(h\nu - E_g)^n \quad (1)$$

where α is the absorption coefficient, h is Planck's constant, ν is the photon frequency, A is the probability parameter for the transition, Eg is the optical bandgap and n related to the transition's type. The optical band gap is obtained from the linear extrapolation of the Tauc plot for P and S thin films. When $(\alpha he)^2$ is plotted against photon energy (hν), the intercept of the straight line on the axis matches to the optical band gap (E.g.). From this plotting, it can be found that the band gap of (S) thin film is (3.2) ev as shown in Fig. 7(a), related to the cerium oxide material and according to the research [8,33], the indirect band gap of CeO_2 is 3.2 eV which matches the above result that is obtained. However, from the Fig. 7(b), which displays the indirect optical energy plotted for the (P3) thin film is (1.7) ev. Therefore, the band gap value decreases for the first and the last photoanodes from (3.2 eV to 1.7 eV). The blue shift in the energy band gap values indicates that the adding of the Cu (NP) and Epolight™ 1178 layers significantly decreases the band gap, leading to enhanced absorption activity that affects the PEC cell performance.

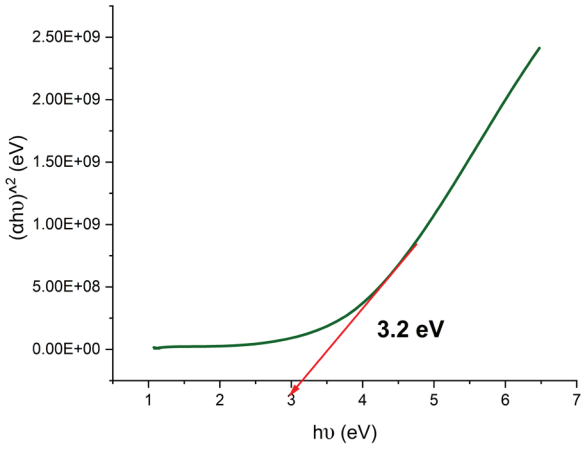

(a)

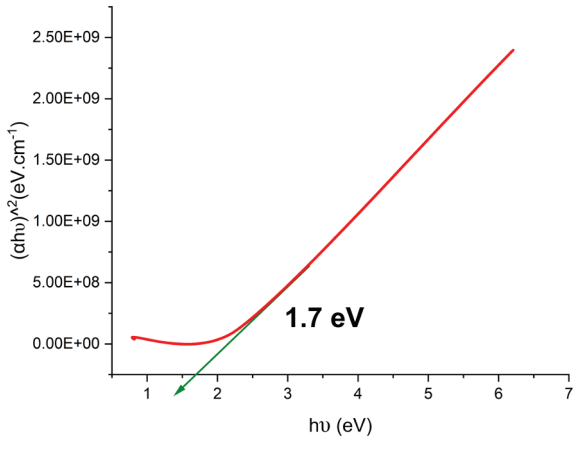

(b)

Fig. 7. The indirect optical energy plotted by Tauc plots: (A) of S, and (B) of P

Photoelectrochemical performances are tested by an electrochemical workstation (ER466, EDAQ company Australia, potentiostat). Ag/AgCl serves as the reference electrode, Pt serves as the counter

Volume 10, Issue 2, December 2024 - ISSN 2356-8569
http://dx.doi.org/10.21622/RESD.2024.10.2.1050

electrode, and the fabricated photoanode (P) [CeO_2(NP)/Cu(NP)/Epolight™1178] serves as the working electrode in the three-electrode system. Regular testing at room temperature uses a 125 mL quartz cell with 2g KOH in DI water (PH 9), which serves as the electrolyte. The linear sweep voltammetry curve is recorded with a scan starting at (0-1) V versus Ag/AgCl under AM 1.5 G illuminations of 100m W.cm^{-2} conditions. J-V curves are obtained at a rate of (100 mW/s) and at a frequency of 20 kHz at the corresponding programme.

The detailed study of the photoanode performance starts by the measurement of dark current, which represents the baseline current in the absence of illumination, to verify that the incident light exclusively causes the observed photocurrent, ensuring it remains unaffected by external influences, and strives for precise evaluations of PEC performance. As a working electrode, (P) photoanode is tested with a scan starting at (0-1) V versus Ag/AgCl in darkness. The recorded dark current density of the P1 working electrode increased from (3.2* 10^{-3} to 5.0 and to 7.6*10 $^{-3}$) mA.cm^{-2} when the Cu (NP) and Epolight™1178 are added as a second and third layer respectively during the thin film fabrication.

The low current observed in the photoanode suggests that there are not numerous defects in the electrode fabrication, which would otherwise cause recombination losses and decreased photoactivity. Due to the differentiation between photocurrent (produced by light-induced processes) and non-photoinduced currents, high dark current may indicate insufficient electrode quality or defective manufacturing, which could have an impact on the PEC cell overall stability and efficiency.

It is decided that one should utilize the comparison principle to achieve the best and most accurate evaluation of the photoelectric response of the designed photoanode. By examining the LED illumination (42 W, Zethors H7) influence on the P photoanode [CeO_2(NP)/Cu(NP)/Epolight™1178] and investigating its behavior, it is found that P exhibites a current density of (34.2) mA.cm^{-2} at 0.99 V vs. Ag/AgCl as displayed in Fig. 8. The positive photogenerated current value indicates that the (P) is an n-type semiconductor [32,34]. This is consistent with CeO_2 status as an n-type semiconductor [8]. It is noteworthy to emphasis that the LED source is used to simulate the full solar spectrum [35], meaning that the results obtained accurately show how this photoanode behaves under solar spectrum characteristics.

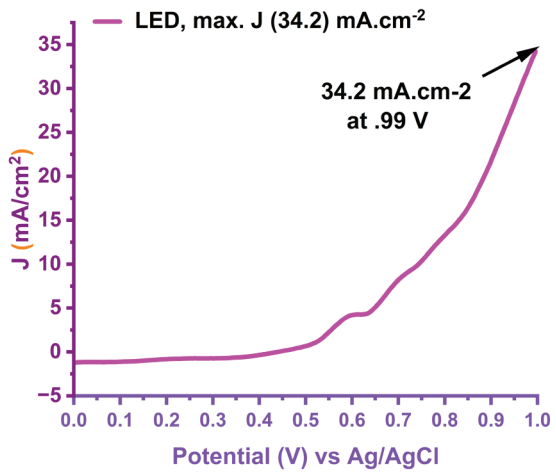

Fig. 8. I-V curve of the P photoanode [CeO_2(NP)/Cu(NP)/Epolight™1178] tested by linear sweep voltammetry under AM 1.5G Illumination of LED source which indicates the max. current density (J) of (34.2) mA.cm^{-2} at 0.99 V vs. Ag/AgCl

It is assumed that a new strategy should be followed to improve hydrogen production through a novel illumination procedure. It includes the simultaneously exposing the P photoanode to **(CW laser sources with the assistance of a UV source instead of a LED or traditional solar simulator sources**). Utilizing that idea, the wavelength of incident light can be matched to the absorption peak of an electrode to achieve maximal absorption. The sources wavelengths are chosen closer to each absorption peak of the (P) photoanode for all regions. To confirm this assumption, three different sources of light are employed simultaneously to illuminate the (P) photoanode [CeO_2(NP)/Cu(NP)/Epolight™1178]. The NIR (980) nm laser, (473) nm laser and the UV source, taking into account its earlier recorded absorption peaks that include the NIR peak at 857 nm as well as the peaks (473, 634) nm at the VIS and UV regions, respectively, as mentioned previously in Fig. 6(a). For the peaks in the visible range, the intensive one is the (473) nm as cleared in Fig. 6(c). Therefore, laser with a suitable wavelength is chosen to match this peak. The sources that are used in this procedure are the CW Diode laser with wavelength of 980 nm (from Shanghai Dream Laser Technology that has an output power of 2W), the DPSS laser (model MBL-FN-473nm-200mW-15050466) with wavelength of 473 nm, and a UV source of 6 W which has a wavelength of around 290 nm. The recorded photocurrent density of the P photoanode increases significantly to (138.3) mA.cm-2 at 0.99 V vs. Ag/AgCl, as can be seen in Fig. 9, which emphasizes the benefits of the photoanode modification and procedure that are employed.

Volume 10, Issue 2, December 2024 - ISSN 2356-8569
http://dx.doi.org/10.21622/RESD.2024.10.2.1050

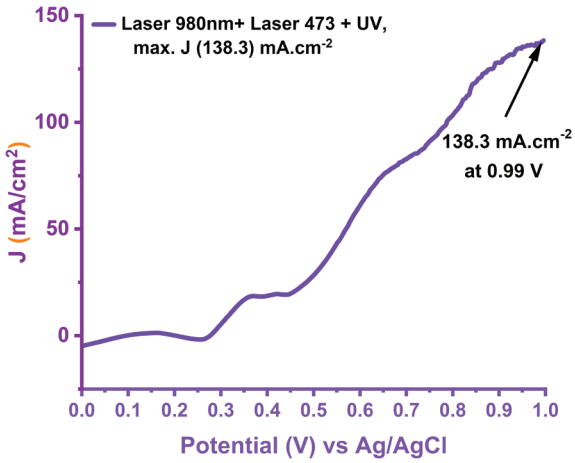

Fig. 9. I-V curve of the P photoanode [CeO_2(NP)/Cu(NP)/ Epolight™1178] tested by linear sweep voltammetry under AM 1.5G Illumination of (980 nm laser+473 nm laser + UV sources simultaneously) which indicates the max. current density (J) of (138.3) mA.cm^{-2} at 0.99 V vs. Ag/AgCl

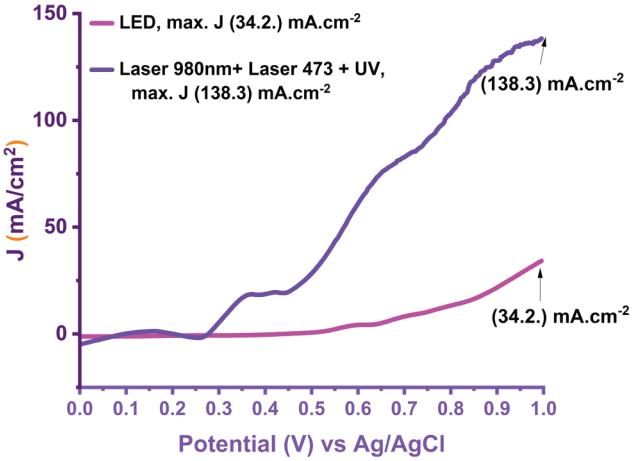

Fig. 10. The comparison in I-V curves of P illuminated by LED source and (980 nm laser+473 nm laser + UV sources simultaneously). The higher current density of (138.3) mA.cm^{-2} V vs. Ag/AgCl recorded to the illumination by laser sources

To unveil the basic reasons of NIR-responsive and full-spectrum-activated photoanode, the cause of dye sensitization must be introduced first. In a review published in 2024, Yuanyong Huang et al. [3] summarize the results of 40 years of recently published research on NIR-activated photocatalysts. The findings are categorized into four areas: dye sensitization, bandgap engineering, plasmonic modification, and up-conversion effects. This is in line with the properties of the Broad IR absorber Epolight™ 1178 dye material, which has a maximum peak at (1073) nm Fig. 4(b) that is used in the fabrication of the P photoanode. This comes in addition to many factors contributed to this rise in current density, including the high conductivity of Cu (NP), the materials nanostructure, which enhance the operative surface area, and the strong SPR effect, which is primarily responsible for the high measured current. The surface plasmon resonance (SPR) effect produced by Cu nanoparticles (NPS) on the dielectric semiconductor CeO_2 extends the light adsorption edge, encourages charge separation, and improves hydrogen generation [8,34,36-38]. On the other hand, the intensive absorption by the CeO_2 nanoparticles layer to the UV source.

Upon comparing the outcome to the LED influence on the same electrode, the extent of the improvement becomes clear as the current density increases from (34.2) mA.cm^{-2} up to (138.3) mA.cm^{-2}, as shown in Fig. 10.

All the above reasons lead to the superior photocurrent density observed, which means that the (P) photoanode demonstrates an excellent activity by performing remarkable and novel result. Through several interrelated mechanisms, laser light improves photoelectrochemical (PEC) cell performance. Because laser sources provide monochromatic, highly coherent light, the illumination wavelength could be precisely selected to match the absorption peaks of the photoanode. When the photoanode is designed to catch light across the UV, VIS, and NIR bands, this guarantees that the greatest number of photons is absorbed. Compared to broadband solar light, lasers can maximize absorption efficiency by targeting specific electronic transitions, leading to more efficient photoexcitation of charge carriers.

The Solar-to-Hydrogen efficiency (η) of all the resulted current densities is presented in Table II and in a 3-electrode PEC configuration when an external bias applying between the working (WE) and the counter electrodes (CE), conversion efficiency is usually evaluated using equation (2) [39, 40]:

$$\eta = [I\,(1.23 - E\ bias)/\ J\ light] \times 100\% \quad (2)$$

Where, (I) is photocurrent density at the given potential observed from the experiment (mA cm^{-2}), E bias is the used potential, 1.23 is the criterion of potential of water splitting, and J light refers the intensity of the irradiating light at 100 mW/cm^2 for AM 1.5 G standard.

TABLE II
THE PHOTOCURRENT DENSITY AT 0.99 V VS. AG/AGCL OF P PHOTOANODE WITH THE ILLUMINATED SOURCES AND THEIR EFFICIENCIES.

Illumination source	Photocurrent density at 0.99 V vs. Ag/AgCl J ($mA.cm^{-2}$)	Solar-to-Hydrogen efficiency (η)
LED	34.2	8.2 %
980 nm Laser + 473 nm Laser + UV source	138.3	33.2 %

The table clearly shows the jump of the photoanode efficiency as it increases from (8.2%) to (33.2%) when illuminated by the new procedure, which is four times more efficient than when it is illuminated by the solar spectrum represented by the LED source.

These results set a new direction for PEC cell optimization by demonstrating the effectiveness of laser-assisted light in boosting hydrogen production, representing a significant step forward in renewable energy research.

IV. CONCLUSIONS

This study demonstrates the transformative potential of laser illumination in enhancing the performance of photoelectrochemical (PEC) cells. By employing a uniquely fabricated photoanode with a tailored dye material, the absorption of light across the UV, VIS, and NIR regions is significantly optimized. The alignment of the laser wavelength with the photoanode absorption peaks enable exceptional photocurrent generation, surpassing the efficiency achieved under conventional solar illumination. Comprehensive structural, compositional, and optical characterizations confirm the high performance of the multi-layered photoanode, highlighting its superior light-harvesting capabilities and catalytic activity. These findings not only underscore the effectiveness of laser illumination in driving PEC processes, but also pave the way for innovative strategies in hydrogen production.

Funding: This research received no external funding.

Conflicts of Interest: The authors declare no conflict of interest.

References

[1] G. Zuher, W. J. Aziz, and R. S. Sabry, "Producing Hydrogen Energy Using Cr2O3-TiO2 Nanocomposite with Animal (Chitosan) Extract via Photocatalaysis," *Ibn AL-Haitham Journal For Pure and Applied Sciences*, vol. 35, no. 4, 2022, doi: 10.30526/35.4.2853.

[2] M. G. C. Zoontjes, "Visible-light-induced water splitting on a chip," University of Twente, Enschede, The Netherlands, 2015. doi: 10.3990/1.9789036538954.

[3] M. Grätzel, "Photoelectrochemical cells," *Nature*, vol. 414, no. 6861, pp. 338–344, Nov. 2001, doi: 10.1038/35104607.

[4] M. B. Costa, M. A. de Araújo, M. V. de L. Tinoco, J. F. de Brito, and L. H. Mascaro, "Current trending and beyond for solar-driven water splitting reaction on WO3 photoanodes," 2022. doi: 10.1016/j.jechem.2022.06.003.

[5] Zainab K. Ali and Mazin A. Mahdi, "Preparation of Silicon Nanowires Photocathode for Photoelectrochemical Water Splitting," *Iraqi Journal of Physics*, vol. 20, no. 4, 2022, doi: 10.30723/ijp.v20i4.1070.

[6] S. Cho, J. W. Jang, K. H. Lee, and J. S. Lee, "Research update: Strategies for efficient photoelectrochemical water splitting using metal oxide photoanodes," *APL Mater*, vol. 2, no. 1, 2014, doi: 10.1063/1.4861798.

[7] A. TROVARELLI, "Catalytic Properties of Ceria and CeO 2 -Containing Materials," *Catalysis Reviews*, vol. 38, no. 4, pp. 439–520, Nov. 1996, doi: 10.1080/01614949608006464.

[8] E. Kusmierek, "A CeO2 semiconductor as a photocatalytic and photoelectrocatalytic material for the remediation of pollutants in industrial wastewater: A review," 2020. doi: 10.3390/catal10121435.

[9] D. Channei, A. Nakaruk, S. Phanichphant, P. Koshy, and C. C. Sorrell, "Cerium Dioxide Thin Films Using Spin Coating," *J Chem*, Jan. 2013, doi: 10.1155/2013/579284.

[10] R. S. Sachit, "Solar cells based on inkjet-printed layer polymer," in *Journal of Physics: Conference Series*, 2021. doi: 10.1088/1742-6596/2114/1/012026.

[11] R. Zamiri *et al.*, "Dielectrical properties of CeO2 nanoparticles at different temperatures," *PLoS One*, vol. 10, no. 4, 2015, doi: 10.1371/journal.pone.0122989.

[12] Y. Tong, W. Liu, C. Li, X. Liu, J. Liu, and X. Zhang, "A metal/semiconductor contact induced Mott-Schottky junction for enhancing the electrocatalytic activity of water-splitting catalysts," 2022. doi: 10.1039/d2se01355j.

[13] F. Mikaeili, T. Gilmore, and P.-I. Gouma, "Photochemical Water Splitting via Transition Metal Oxides," *Catalysts*, vol. 12, no. 11, p. 1303, Oct. 2022, doi: 10.3390/catal12111303.

[14] S. S. Martín, M. J. Rivero, and I. Ortiz, "Unravelling the mechanisms that drive the performance of photocatalytic hydrogen production," 2020. doi: 10.3390/catal10080901.

[15] M. C. Crisan, M. Teodora, and M. Lucian, "Copper nanoparticles: Synthesis and characterization, physiology, toxicity and antimicrobial applications," 2022. doi: 10.3390/app12010141.

[16] H. S. Cho, T. Kodama, N. Gokon, S. Bellan, and J. K. Kim, "Development of synthesis and fabrication process for mn-ceo2 foam via two-step water-splitting cycle hydrogen production†," *Energies (Basel)*, vol. 14, no. 21, 2021, doi: 10.3390/en14216919.

[17] M. B. Gawande *et al.*, "Cu and Cu-Based Nanoparticles: Synthesis and Applications in Catalysis," *Chem Rev*, vol. 116, no. 6, pp. 3722–3811, Mar. 2016, doi: 10.1021/acs.chemrev.5b00482.

[18] P. Zhang, H. Liu, and X. Li, "Photo-reduction synthesis of Cu nanoparticles as plasmon-driven non-semiconductor photocatalyst for overall water splitting," *Appl Surf Sci*, vol. 535, 2021, doi: 10.1016/j.apsusc.2020.147720.

[19] F. G. Hamzah and H. R. Humud, "Signature of plasmonic nanostructures synthesised by electrical exploding wire technique on surface-enhanced raman scattering," *Iraqi Journal of Science*, vol. 62, no. 1, 2021, doi: 10.24996/ijs.2021.62.1.16.

[20] M. Watanabe, "Dye-sensitized photocatalyst for effective water splitting catalyst," 2017. doi: 10.1080/14686996.2017.1375376.

[21] M. Raffi *et al.*, "Investigations into the antibacterial behavior of copper nanoparticles against Escherichia coli," *Ann Microbiol*, vol. 60, no. 1, 2010, doi: 10.1007/s13213-010-0015-6.

[22] D. Han, Z. Meng, D. Wu, C. Zhang, and H. Zhu, "Thermal properties of carbon black aqueous nanofluids for solar absorption," *Nanoscale Res Lett*, vol. 6, no. 1, p. 457, Jul. 2011, doi: 10.1186/1556-276X-6-457.

[23] A. Kaliyaraj Selva Kumar, Y. Zhang, D. Li, and R. G. Compton, "A mini-review: How reliable is the drop casting technique?," 2020. doi: 10.1016/j.elecom.2020.106867.

[24] M. Wu, A. H. Caldwell, and A. Allanore, "Surface Tension of High Temperature Liquids Evaluation with a Thermal Imaging Furnace," 2019, pp. 33–41. doi: 10.1007/978-3-030-06143-2_4.

[25] P. Ravi and J. Noh, "Photocatalytic Water Splitting: How Far Away Are We from Being Able to Industrially Produce Solar Hydrogen?," 2022. doi: 10.3390/molecules27217176.

[26] D. Girija, H. S. B. Naik, cn Sudhamani, and B. V. Kumar, "Cerium Oxide Nanoparticles-a Green, Reusable, and Highly Efficient Heterogeneous Catalyst for the Synthesis of Polyhydroquinolines Under Solvent-free Conditions," vol. 3, pp. 373–382, 2011.

[27] Y. Fan, D. Li, M. Deng, Y. Luo, and Q. Meng, "An overview on water splitting photocatalysts," *Frontiers of Chemistry in China*, vol. 4, no. 4, 2009, doi: 10.1007/s11458-009-0100-1.

[28] M. C. Crisan, M. Teodora, and M. Lucian, "Copper Nanoparticles: Synthesis and Characterization, Physiology, Toxicity and Antimicrobial Applications," *Applied Sciences*, vol. 12, no. 1, p. 141, Dec. 2021, doi: 10.3390/app12010141.

[29] J. Li and N. Wu, "Semiconductor-based photocatalysts and photoelectrochemical cells for solar fuel generation: A review," 2015. doi: 10.1039/c4cy00974f.

[30] S. Cho, J.-W. Jang, K.-H. Lee, and J. S. Lee, "Research Update: Strategies for efficient photoelectrochemical water splitting using metal oxide photoanodes," *APL Mater*, vol. 2, no. 1, Jan. 2014, doi: 10.1063/1.4861798.

[31] S. Bai *et al.*, "An Integrating Photoanode of WO3/Fe2O3 Heterojunction Decorated with NiFe-LDH to Improve PEC Water Splitting Efficiency," *ACS Sustain Chem Eng*, vol. 6, no. 10, 2018, doi: 10.1021/acssuschemeng.8b02267.

[32] W. Ismail, G. Ibrahim, M. A. Habib, O. K. Alduaij, M. Abdelfatah, and A. El-Shaer, "Advancement of Physical and Photoelectrochemical Properties of Nanostructured CdS Thin Films toward Optoelectronic Applications," *Nanomaterials*, vol. 13, no. 11, 2023, doi: 10.3390/nano13111764.

[33] S. Soni *et al.*, "Electronic Structure and Room Temperature Ferromagnetism in Gd-doped Cerium Oxide Nanoparticles for Hydrogen Generation via Photocatalytic Water Splitting," *Global Challenges*, vol. 3, no. 5, 2019, doi: 10.1002/gch2.201800090.

[34] M. L. Gaur, P. P. Hankare, K. M. Garadkar, S. D. Delekar, and V. M. Bhuse, "CdSe thin films: morphological, optoelectronic and photoelectrochemical studies," *Journal of Materials Science: Materials in Electronics*, vol. 25, no. 1, pp. 190–195, Jan. 2014, doi: 10.1007/s10854-013-1572-9.

[35] Y. Huang, H. Yang, X. Lu, M. Chen, and W. Shi, "Near infrared-driven photocatalytic overall water splitting: Progress and perspective," 2024. doi: 10.1016/S1872-2067(23)64594-2.

[36] M. A. Hamid, Y. Zengin, and I. Boz, "Surface Plasmon Resonance-enhanced photocatalytic water-splitting for improved visible-light-driven H2 generation using Ag-modified twin crystal Cd0.5Zn0.5S photocatalysts," *Catal Commun*, vol. 187, 2024, doi: 10.1016/j.catcom.2024.106841.

[37] S. Khanam and S. K. Rout, "Plasmonic Metal/Semiconductor Heterostructure for Visible Light-Enhanced H 2 Production," *ACS Omega*, vol. 7, no. 29, pp. 25466–25475, Jul. 2022, doi: 10.1021/acsomega.2c02459.

[38] S. Wang *et al.*, "Boosting photoelectrochemical water splitting by Au@Pt modified ZnO/CdS with synergy of Au-S bonds and surface plasmon resonance," *J Catal*, vol. 408, 2022, doi: 10.1016/j.jcat.2022.03.003.

[39] L. Liu, C. Zhao, J. Xu, and Y. Li, "Integrated CO2 capture and photocatalytic conversion by a hybrid adsorbent/photocatalyst material," *Appl Catal B*, vol. 179, 2015, doi: 10.1016/j.apcatb.2015.06.006.

[40] Y. Qiu *et al.*, "Current progress in developing metal oxide nanoarrays-based photoanodes for photoelectrochemical water splitting," *Sci Bull (Beijing)*, vol. 64, no. 18, pp. 1348–1380, Sep. 2019, doi: 10.1016/j.scib.2019.07.017.